JOURNAL OF SPACECRAFT AND ROCKETS
Vol. 34, No. 5, September–October 1997

Some Correlation Techniques for Environmentally Induced Anomalies Analysis

F. J. López Honrubia* and A. Hilgers†
European Space Agency, Noordwijk NL-2200 AG, The Netherlands

The possible environmental origin of a small group of anomalies observed on two satellites of the European Space Agency series, Meteosat, is investigated by using both linear and nonlinear classification methods of the environmental data measured onboard the Geosynchronous Operational Environmental Satellites of the National Oceanic and Atmospheric Administration. The techniques developed for this study appear as powerful tools for investigating quantitatively the relationships between the environment data and the occurrence of the anomalies in spite of the small size of the anomaly data set. Moreover, the result of the study suggests that not only the fluence of energetic electrons but also the time variation of the flux over several days has an influence on the anomaly occurrence.

Nomenclature

A = time series of the values of F_D preceding a day with an anomaly
B = time series of the values of F_D preceding a day without an anomaly
F_D = daily averaged flux of electrons with energy above 2 MeV, $cm^{-2}s^{-1}sr^{-1}$
M_A = total number of patterns of type A
N = window interval (in days) of the times series A or B
q = ratio of patterns classified as being of type A
q' = ratio of correctly classified patterns of type A
Π = probability of a random process to do better than q'

Introduction

ENVIRONMENTALLY induced spacecraft anomalies have recently been the topic of a special section of the *Journal of Spacecraft and Rockets*.[1] Spacecraft anomalies of this kind can be defined as such if they are anomalous behavior of the spacecraft without apparent onboard origin. However, it is very difficult to unambiguously identify the environmental cause of an operational anomaly for two main reasons. First, the information on the space environment is not always available. Second, the knowledge of the exact physical properties of the spacecraft material, especially after exposure to the space environment, is often insufficient to properly model the process suspected to cause an anomaly. Therefore, the most convincing studies rely on statistical correlations between anomaly events and the environmental parameters.

Most of the time, environmentally induced anomalies present no threat to spacecraft missions and are easily corrected by remote control. However, they represent an annoyance to the operations staff and sometimes can lead to a major problem. In 1994 the Canadian communication satellites ANIK E1 and E2 both failed because of problems with their momentum wheel control systems. The cost of their recovery and of the reduction in their lifetimes, estimated at tens of millions of dollars, evidenced how important the effect of the plasma environment on spacecraft can be. These anomalies are suspected to be of electrical origin and related to the space plasma environment.[2]

There are two major mechanisms usually cited for explaining the operational anomalies due to the plasma environment: surface charging[3,4] and bulk charging.[5,6] Surface charging results from the buildup of electrostatic charges on material surfaces exposed to the plasma. If the surface is nonhomogeneous and has a complicated geometry, strong electric fields may be created at some location of the surface. This can result in breakdown of the electrostatic configuration accompanied by powerful current transients that are induced or conducted into sensitive electronics. The electrostatic distribution equilibrium on spacecraft surfaces following change in the space environment is usually reached on a time scale on the order of 10^{-3} s to 1 min. The most significant environmental parameters are the sunlit area, the energy distribution of the electron population, and the total plasma density.

In the bulk charging process, the charge buildup occurs behind spacecraft surfaces, e.g., within dielectric coating material, and is due to electrons with energy sufficient to penetrate the typical thickness on the spacecraft surfaces, i.e., energy on the order of 100 keV to 1 MeV. The resulting electrostatic field in some locations can be very large if the electric conductivity is too low to allow a rapid leakage of the charge deposited by the penetrating electrons. The time scale for the buildup of the electrostatic configurations until a breakdown occurs can be several days.

For both mechanisms, only the charging processes are rather well understood and quantitative modeling of them feasible. The process by which the equilibrium, or quasiequilibrium, of the electrostatic configuration breaks down is still not completely understood and is a matter of debate. As a consequence, criteria for the protection of systems against electrostatic breakdown are largely empirical. The plasma parameters relevant to both surface and bulk charging may vary by orders of magnitude in geosynchronous orbit on a day time scale. The dynamics of this environment is still a research topic.

In the last few decades there have been several studies indicating correlation between spacecraft anomalies and large negative surface charging.[4,7] As a consequence, spacecraft designers now include specifications to control surface charging either by grounding or by a judicious choice of surface materials that charge moderately even in severe environments.[8] Recently, however, there has been evidence of correlation of some operational anomalies with enhanced flux of very high energy electrons, i.e., with energy on the order of a few mega electron volts.[2,5,6,9–11] Studies relying on dedicated spacecraft experiments, e.g., CRRES[10] and SCATHA,[11] have led to the most reliable proofs of the existence in space of bulk-charging-induced anomalies. However, the design of these spacecraft was purposely far less conservative than that of the commercial satellites. Conversely, studies involving commercial satellites are limited by the small anomaly data set and the lack of information on the environment and therefore suffer from poor statistics. To overcome part of these difficulties, Wrenn[2] studied the correlation of anomalies observed on a commercial geosynchronous satellite with particle measurements provided by other spacecraft, e.g., GOES-7, at the same orbit. This study gave further evidence of the existence of bulk-charging-induced anomalies on commercial spacecraft, but statistics were still poor.

Received May 22, 1996; revision received Feb. 28, 1997; accepted for publication April 26, 1997.

*Engineer, European Space Research and Technology Centre.
†Physicist, European Space Research and Technology Centre.

The present study was performed to seek a possible correlation between the orbital environment and a group of anomalies observed on two operational spacecraft that had no apparent onboard origin. Because the anomaly data set was very small (40 events) and the environment data were obtained from satellites at another location, the quantitative assessment of the correlation was challenging and required careful tests of the accuracy of the methods used. The paper focuses on the methods of correlation developed for this study, which are based on a classification of the environmental data. A detailed analysis of the mechanism by which the anomalies occur is beyond the scope of this paper.

The paper is organized as follows. After a short description of the data sets, a classical method of descriptive statistics is used to evaluate the probability of occurrence of anomalies as a function of the daily averaged flux. To gain more insight into the characteristics of the environment prevailing when the anomalies occur, a linear classification method of the environmental data is applied. Finally, a nonlinear method, which generalizes the classification using nonlinear decision boundaries and a nonscalar description of the environment, is applied, and the results are discussed.

Data

The anomaly data set used for this study corresponds to a group of anomalies affecting two consecutive Meteosat spacecraft, MOP-1 and MOP-2. They are characterized by a timed command not being generated onboard the spacecraft at the expected time that could not be explained as software or command errors. They could be related to a spurious onboard generated register reset. Other operational anomalies have been observed on previous Meteosat spacecraft, and the result of the corresponding analyses reported elsewhere.[9]

For the purpose of this study, only the date of the anomaly is of interest. The anomaly data set consists of the days when there had been one or more time-tag anomalies on at least one of the two Meteosat satellites. The period covers five years of operation. MOP-1 was operational from mid-1989 and was replaced by MOP-2 in February 1994. No change in anomaly occurrence behavior has been observed from one spacecraft to the other.

The data of the high energy electron environment are provided by the U.S. series of Geosynchronous Operational Environmental Satellite (GOES) spacecraft of the National Oceanic Atmospheric Administration. The parameter chosen to describe the environment is the daily averaged flux of electrons with energy above 2 MeV, F_D. The choice of daily averaged data was motivated by the fact that the GOES satellites and the Meteosat satellites are at different longitudes. Therefore, comparison of the environment experienced by these two types of satellite can be done only with data averaged over at least one day.

The data over the investigated period are displayed in Fig. 1. The vertical lines in the upper panel indicate the days when one or more anomalies occur. The mean daily electron flux is displayed in the lower panel. The strong variability of the electron density flux appears clearly, the range of variation covering more than four orders of magnitude. The purpose of the next sections is to seek a quantitative relationship between these two sets of data.

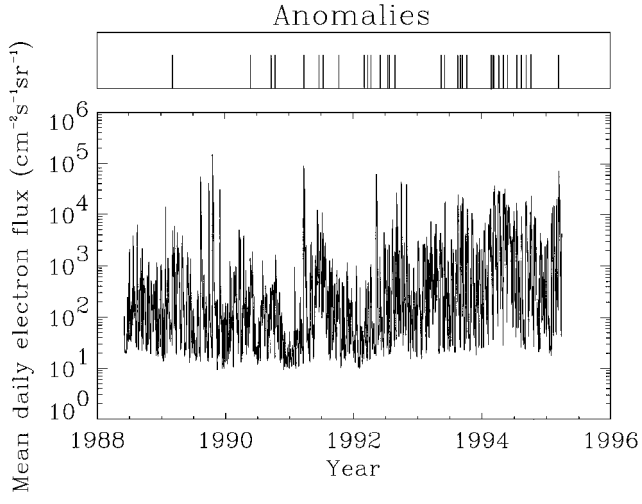

Fig. 1 Daily averaged flux of electrons above 2 MeV measured by GOES satellites over the investigated period. The days when an anomaly occurred are indicated in the top panel.

Statistical Description

There are several approaches for extracting quantitative information from these data. Because the number of anomalies is small, the identification of some characteristics prevailing in the period of time preceding an anomaly could be expected from a one-by-one inspection of the time series of the daily averaged flux. The daily averaged flux is shown in Fig. 2 as a function of the number of days before an anomaly occurs for two different events: anomaly of day 22-6-1991 (top panel) and anomaly of day 23-7-1994 (bottom panel). These two time series appear to be very different from each other regarding both their overall profile and the order of the magnitude around the day preceding the anomaly. This lack of obvious common features between two samples shows that a statistical treatment is necessary.

The histogram of the distribution of the daily averaged electron flux over the period of interest is shown in Fig. 3 for the day preceding an anomaly (top panel) and for all events (bottom panel). Although the two distributions overlap, there is a clear trend for the anomalies to occur during days with high-flux values. This relationship can be quantified by the probability of an anomaly to occur as a function of the flux level (Fig. 4, top panel). Because the data set is small, this probability distribution is dropping to zero in many bins of the flux level scale. If one discards these bins, the overall aspect of the variation of the preceding probability confirms that the anomaly occurrence increases with the flux level. The highest probability is around 50% when the flux is between 4.0×10^4 and 6.3×10^4 $cm^{-2}s^{-1}sr^{-1}$. Similar quantitative information is provided by the cumulated probability of an anomaly occurrence for the flux above

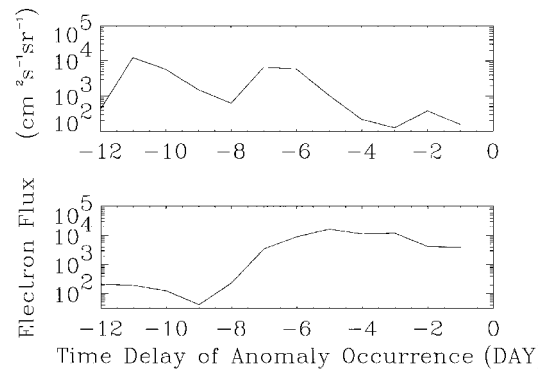

Fig. 2 Time series of the daily averaged flux of electrons above 2 MeV preceding the anomaly events of 22-6-1991 (top panel) and 23-7-1994 (bottom panel). Day 0 is a day when an anomaly occurred.

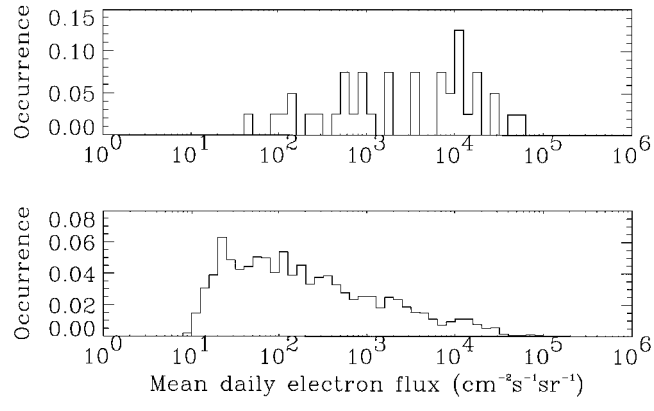

Fig. 3 Histogram of the distribution of the daily averaged electron flux over the period of interest for the day preceding an anomaly (top panel) and for all events (bottom panel).

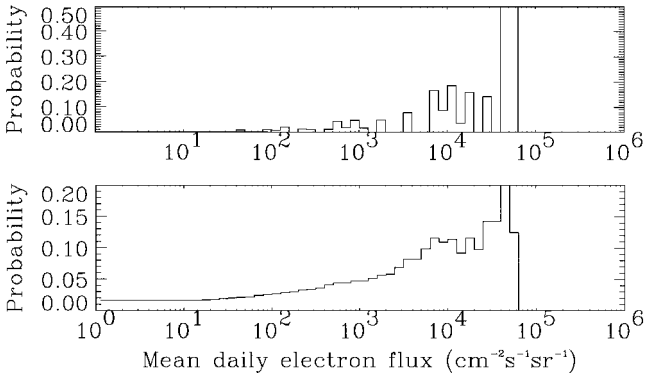

Fig. 4 Probability of an anomaly to occur as a function of the flux level (top panel) and cumulated probability of an anomaly occurrence for the flux above a given threshold (bottom panel).

a given threshold (Fig. 4, bottom panel). The two preceding statistical descriptions, however, do not provide any specific information to distinguish the days with an anomaly from the days without an anomaly.

Classification as a Correlation Method

Further insight into the anomaly process could be obtained from a criterion on the environment able to discriminate the days with anomalies and the days without. Because the preceding distributions show an accumulation of anomaly events in the high-flux range and of days without anomaly in the low-flux range, a natural criterion would be a flux threshold separating the flux domain where most anomalies occur. This approach is typical of classification methods making use of a linear decision boundary. The classification applies to the value of F_D. In the following, the two classes that need to be discriminated are labeled A when associated to an anomaly and B when not. Furthermore, for consistency with the nomenclature used in classification theory, the elements of the classes are called patterns. The efficiency of the classification is determined by the ratio of correctly classified patterns of each class.

In the beginning of this study, only one scalar parameter is used to describe the environment, i.e., F_D. The decision boundary is therefore a threshold value. Patterns with values below this threshold will be classified as belonging to class B, whereas patterns with values above it will be classified as belonging to class A. From the examination of Fig. 3, it can be seen that the two classes are never completely separated on the basis of a threshold on the daily averaged flux. This overlapping is due to the fact that the occurrence of anomalies depends on factors other than merely the averaged electron flux over one day. These factors might be related to some parameters characteristic of the system or of the environmental conditions.

The success of the classification for classes A and B as a function of the threshold is shown in Fig. 5. Because the two classes overlap, the two curves cannot reach unity, i.e., 100% success of classification, for the same value of the threshold. Obviously, the unity is reached for class A when the threshold is below the lowest flux associated to an anomaly and for class B when the threshold is above the highest flux observed during a day without an anomaly. Determining the threshold value that separates best the classes is somewhat arbitrary and depends on the purpose of such a classification. In the following, the best separation is assumed to be the one corresponding to the maximum of the sum of the ratios of correctly classified patterns A and B. In the present case, the sum of the two ratios (not shown on the graph) is maximum where the two curves cross each other, i.e., for a flux equal to 7×10^2 cm^{-2}s^{-1}sr^{-1}. Both ratios of correctly classified patterns are equal to 73% for this threshold.

The significance of this result is worth investigating quantitatively. Formally, the preceding classification method leads to the fact that a ratio q of the patterns is classified as belonging to class A. The ratio of correctly classified patterns A is $q' = 0.73$. The probability of q' to be obtained by chance can be evaluated through the derivation of the probability Π that a random process with a probability q to classify any pattern in class A leads to a ratio of

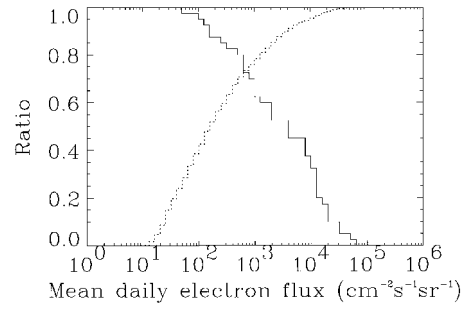

Fig. 5 Ratios of correctly classified patterns of class A (anomaly; ——) and B (no anomaly; ·····) as a function of the threshold.

success for A patterns greater than or equal to q'. One can show that this probability is

$$\Pi = \sum_{k=q'M_A}^{M_A} \frac{M_A!}{k!(M_A-k)!} q^k (1-q)^{(M_A-k)} \qquad (1)$$

Replacing q and q' by their quantitative values, one obtains Π on the order of 10^{-9}, which is a very small number and indicates that the level of significance of the correlation is very high.

Another important test of the significance of the classification is its ability to operate on previously unseen data. This test can be performed by dividing the data into two sets: a reference set, which is used to derive the classification rule such as to maximize the sum of the ratios of the correctly classified patterns, and a test set, which is used to evaluate the efficiency of the classification on previously unseen data. The division was done at random with the only constraint that each set contains half of patterns A and half of patterns B. This constraint ensures that there are enough patterns to find a reliable quantitative relationship between the environment data and the anomalies as well as to test this relation with previously unseen patterns. This operation was repeated 20 times such that information on the dispersion of the results can be obtained. The average ratio of correctly classified patterns of the test set was found to be equal to 0.76 for patterns A and 0.70 for patterns B, whereas the standard deviations were, respectively, 0.09 and 0.03. The difference between both values of the standard deviation is simply explained by the relatively low number of patterns of class A in both the reference and the test data sets compared with the number of patterns of class B. While using this reduced set of data, one obtains values of Π typically on the order of 10^{-4}, which is still low and attests to a high confidence level.

To summarize the results of this section, quantitative evidence has been given of a strong correlation between the value of F_D and the occurrence of an anomaly the following day. Furthermore, a flux threshold can be determined by a linear classification method that provides a general rule able to discriminate $76 \pm 12\%$. However, the ratio of false alarm over the ordinary day is then about 30%. The value of Π averaged over 20 random selections of a pair of reference and test sets can be taken as a measure of the level of the correlation between the anomaly data set and the environmental parameters considered. This value takes into account both the significance level of the correlation and the ability to generalize the relationship derived from the classification rule to unseen data.

Flux Averaged over Several Days

In the preceding sections, evidence for correlation between the anomaly occurrence and the value of F_D the day preceding the events has been demonstrated, and its significance level quantitatively assessed. In this section, a parametric study is performed to determine whether better correlation is obtained when the electron flux is averaged over more than one day. The same technique as described earlier is used to provide a measure of the level of the correlation.

In Fig. 6 the mean value of the ratios of correctly classified patterns A (top panel) and patterns B (bottom panel) of the test data is displayed as a function of the number of days over which the flux was averaged. The error bars correspond to the standard deviation.

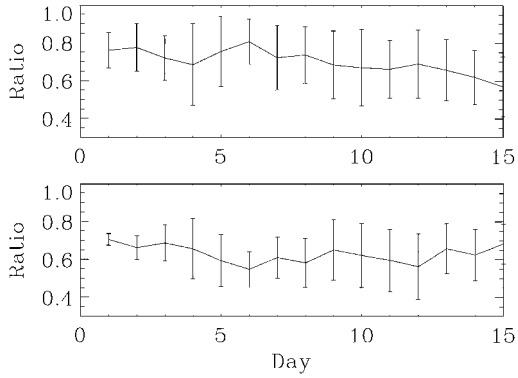

Fig. 6 Mean values and standard deviations of the ratios of correctly classified patterns *A* (anomaly; upper panel) and patterns *B* (no anomaly; lower panel) as a function of the window length over which the flux is averaged.

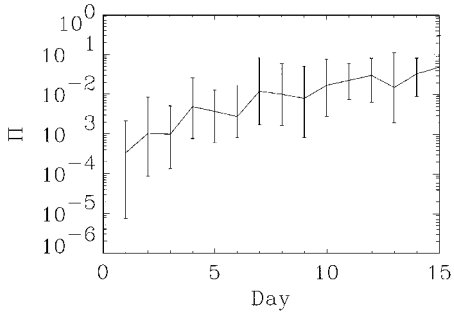

Fig. 7 Mean value and standard deviation of the probability of a random process to perform as well as the linear classification as a function of the window length over which the flux is averaged.

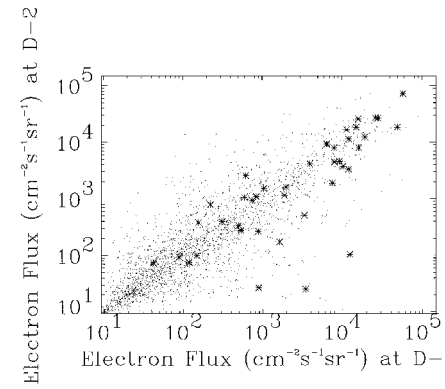

Fig. 8 Distribution of the patterns of class *A* (anomaly; ∗) and class *B* (no anomaly; ·) for *N* = 2 as a function of the daily averaged flux two days before an anomaly occurred (*D* − 2) and one day before an anomaly occurred (*D* − 1).

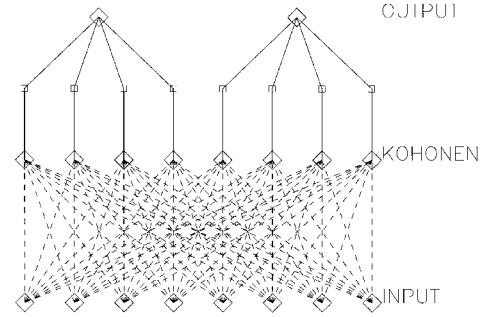

Fig. 9 Sketch of an LVQ neural network used for a classification of vectors of eight dimensions in two classes, making use of four prototypes per class (see text for explanation).

The overall profile does not indicate any particular trend of the variation of the ratios of correctly classified patterns with the window length, except that the two ratios seem to have opposite variation. This fact can be understood because a good ratio of correctly classified patterns *A* is mainly obtained at the expense of a bad ratio of correctly classified patterns *B*. A parameter free from this effect is the probability Π described earlier and shown in Fig. 7 as a function of the number of days over which the flux is averaged. One can see that the overall trend is that Π increases with the window length, indicating a decrease of the performance of the classification and therefore of the level of correlation. The best correlation appears to be obtained when the flux data are averaged over one day.

Nonlinear Classification of Nonscalar Patterns

In this section the correlation between anomaly occurrence and the environment based on the classification technique is performed using time series of F_D instead of merely a scalar value. The time series with window length equal to N days can be considered as vectors of a space of dimension N. An example of the distribution of nonscalar patterns of class A ($*$) and of class B ($\cdot$) when N equals 2 is shown in Fig. 8. In this case, the linear decision boundary would be a straight line. As for $N = 1$, however, it can be seen that, whatever the line chosen, the two classes will not be entirely separated. A linear classification that separates entirely the two classes might be found for N large enough. However, it is not necessary to constrain the classification to rely on a linear decision boundary, i.e., a hyperplane with dimension $N - 1$. More general boundaries, e.g., broken hyperplanes or closed hypersurfaces, could be more efficient. Such a more general classification is performed in the following for various values of N.

The method used for this study relies on a learning vector quantization (LVQ) neural network available in a commercial software package.[12] An LVQ neural network consists of an input layer, a hidden layer, and an output layer. The input layer is composed of as many neurons as input parameters, i.e., N. The output layer contains one node for each of the two classes. The hidden layer, commonly referred to as the Kohonen layer, learns and performs the classification task. A sketch of an LVQ neural network is shown in Fig. 9 for $N = 8$. Once tuned through the LVQ algorithm described next, the weights connecting the input nodes to each neuron in the Kohonen layer constitute the prototype vectors representative of the training data set. Classification of a new pattern is performed by determining the class to which the closest prototype vector belongs. In this study, four prototypes for each class were used. Some trials with more prototypes did not lead to a better classification.

The basic LVQ algorithm is as follows. In the learning phase, for each training pattern, the distance to each prototype (or weight) vector is computed, and the closest prototype is declared to be the winner. If the winning prototype and the training pattern belong to the same class, the prototype is moved toward the training pattern through modifying the weights by an amount that must be arbitrarily decided; otherwise it is moved away from the training pattern. In the operational phase, the distance of a pattern to each prototype is computed, and again the closest prototype is declared to be the winner, but, of course, no more update of the prototypes is done. The input is then assigned to the class to which the winning prototype belongs. A more detailed description of the LVQ algorithm can be found in most of the neural network textbooks.

In the same way as with the linear classification technique, the level of the correlation between the anomaly data set and the environmental data is estimated through the procedure consisting of performing the classification task of patterns A and B using 20 different random selections of a reference set and a test set. Furthermore, a parametric study of the correlation is performed, with the window length N varying from 2 to 12 days.

The mean value and the standard deviation as a measurement of the dispersion of the ratios of correctly classified patterns of class A and B, respectively, are displayed in Fig. 10 as a function of N. The corresponding value of Π is displayed in Fig. 11. As previously observed with the linear classification (see, for example, Fig. 6), the two ratios of correctly classified patterns vary in a symmetric way, indicating that a good success ratio for patterns A is mainly obtained at the expense of a bad success ratio for patterns B. The only exception in the studied range is for $N = 8$, where a local maximum

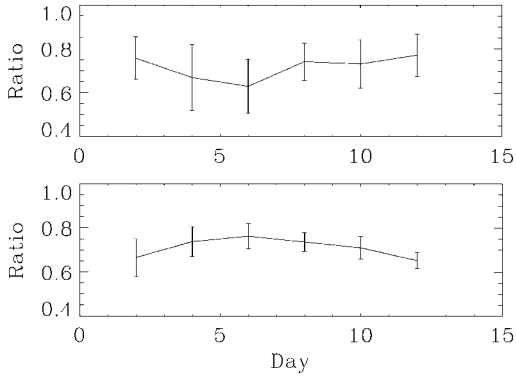

Fig. 10 Mean values and standard deviations of the ratios of correctly classified patterns *A* (anomaly; upper panel) and patterns *B* (no anomaly; lower panel) as a function of the window length of the time series.

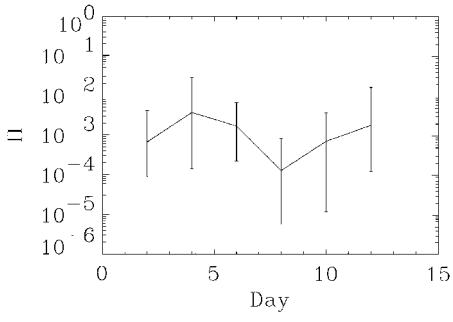

Fig. 11 Mean value and standard deviation of the probability of a random process to perform as well as the LVQ neural network for each window length investigated.

of the ratio of correctly classified patterns A is not associated with any local minimum of the ratio of correctly classified patterns B. The particular behavior for $N = 8$ is even more striking in Fig. 11, where one can see that Π reached for this value a minimum about one order of magnitude lower than the other points for which computation was performed. This feature is interpreted as a maximum of the correlation between the anomaly events and the environmental patterns with respect to the window length of the time series of F_D.

Discussion

At the current stage of this study, it is not clear what the characteristic features of the time series preceding an anomaly are and how they relate to the anomaly generation mechanism. The result, however, suggests that the electron fluence over a given number of days alone is not necessarily the best environmental index to measure anomaly risk occurrence and a refined index could be found by taking into account change of the daily averaged flux over several consecutive days. It must be understood that the preceding results are still compatible with the bulk charging/discharging mechanism as a cause of the anomalies because the instantaneous flux and its time variation may have an indirect but significant effect by affecting the conductivity of the material and may be the discharge triggering mechanism, whereas the fluence can be directly related to the charge accumulation within dielectrics. The fact that the flux dynamics play a significant role in the anomaly occurrence is of importance not only for the understanding of the mechanism at the origin of the anomaly but also for the refinement of the models (empirical and physically based) of the hazardous energetic electron environment to be used for spacecraft engineering purposes.[13]

Moreover, because the daily averaged electron flux on the day when the anomaly occurs was excluded from the input, the classifications can be considered to be forecast systems.[14,15] The input of such systems is a time series of the daily averaged flux, and the output is a value indicating whether an anomaly will occur the day after. The success ratio at this stage, typically 75% in anomaly forecast but at the expense of 25% false alarms, is still too low for most operational purposes. However, some improvement could be achieved by refining the description of the environment, either by including the local time, which has sometimes been found to be a determinant parameter, or by studying the influence of the energy ranges on the results.[9]

Conclusion

In this study, a method was developed to quantify the correlation between anomaly occurrence and environmental data. It has been shown that a strong correlation exists between the daily averaged flux of electrons above 2 MeV energy, as measured on GOES satellites, and a series of anomalies observed on two Meteosat satellites, although they are located at a different longitude. Furthermore, a parametric study of the significance level of the correlation indicated that an important part of the information on the environmental conditions prevailing before anomaly occurrence is contained in the fluence received the day preceding the anomaly and in the dynamics of the daily averaged flux over the preceding eight days.

Acknowledgments

The work of F. J. López Honrubia was possible thanks to the Spanish Young Graduate Training Program held by the European Space Agency and the Spanish Ministry of Industry and financially supported by the Spanish Ministry of Education and Science. We wish to express our thanks to J. Fuchs for his advice and support in the use of the neural network software. The idea of using neural network techniques for the purpose of identifying a correlation between spacecraft anomalies and the high-energy electron environment was suggested by E. Daly. We are grateful to R. O. Salisbury for having provided the data and information about anomalies and to F. Camermans for having prepared the data in a format suitable to this analysis. Useful comments and suggestions from both reviewers and the associate editor are acknowledged.

References

[1]Lauriente, M., and Gaudet, J., "Environmentally Induced Spacecraft Anomalies," *Journal of Spacecraft and Rockets*, Vol. 31, No. 2, 1994, p. 153.

[2]Wrenn, G. L., "Conclusive Evidence for Internal Dielectric Charging Anomalies on Geosynchronous Communications Spacecraft," *Journal of Spacecraft and Rockets*, Vol. 32, No. 3, 1995, pp. 514–520.

[3]De Forest, S. E., "Spacecraft Charging at Synchronous Orbits," *Journal of Geophysical Research*, Vol. 77, Feb. 1972, pp. 561–569.

[4]Fredricks, R. W., and Scarf, F. L., "Observation of Spacecraft Charging, Effects in Energetic Plasma Regions," *Photon and Particle Interactions with Surface in Space*, D. Reidel, Dordrecht, The Netherlands, 1973, pp. 277–308.

[5]Leung, P., Whittlesey, A. C., Garrett, H. B., and Robinson, P. A., "Environment-Induced Electrostatic Discharges as the Cause of Voyager 1 Power-On Resets," *Journal of Spacecraft and Rockets*, Vol. 23, No. 3, 1986, pp. 323–330.

[6]Vampola, A. L., "Thick Dielectric Charging on High Altitude Spacecraft," *Journal of Electrostatics*, Vol. 20, Jan. 1987, pp. 21–30.

[7]Wrenn, G. L., "Surface Charging of Spacecraft in Geosynchronous Orbit," *The Behaviour of Systems in the Space Environment*, edited by R. N. de Witt, D. P. Duston, and A. K. Hyder, Kluwer, Dordrecht, The Netherlands, 1993, pp. 491–511.

[8]Purvis, C. K., Garrett, H. B., and Whittlesey, A. C., "Design Guidelines for Assessing and Controlling Spacecraft Charging Effects," NASA TP-2361, Oct. 1984.

[9]Rodgers, D. J., "Correlation of Meteosat-3 Anomalies with Data from the Spacecraft Environment Monitor," European Space Agency, EWP-1620, Noordwijk, The Netherlands, June 1991.

[10]Violet, M. D., and Frederikson, A. R., "Spacecraft Anomalies on the CRRES Satellite Correlated with the Environment and Insulator Samples," *IEEE Transactions on Nuclear Science*, Vol. 40, No. 6, 1993, pp. 1512–1520.

[11]Koons, H. C., and Gorney, D. J., "Relationship Between Electrostatic Discharges on Spacecraft P78-2 and the Electron Environment," *Journal of Spacecraft and Rockets*, Vol. 28, No. 6, 1991, pp. 683–688.

[12]"Neural Computing, A Technology Handbook for Professional II/PLUS and Neural-Works Explorer," NeuralWare, Inc., Pittsburgh, PA, 1993, pp. 227–233.

[13]Tascione, T., and Cliffswallow, W., "The National Space Weather Program," AIAA Paper 95-0550, Jan. 1995.

[14]Maynard, N. C., "Space Weather Prediction," *Reviews of Geophysics*, Supplement, July 1995, pp. 547–557.

[15]Joselyn, J. A., "Geomagnetic Activity Forecasting: The State of the Art," *Reviews of Geophysics*, Vol. 33, No. 3, 1995, pp. 383–401.

A. C. Tribble
Associate Editor